Available online at www.sciencedirect.com
ScienceDirect
Electrochimica Acta 53 (2008) 6740–6752
ELECTROCHIMICA Acta
www.elsevier.com/locate/electacta

A molecular theory of chemically modified electrodes with self-assembled redox polyelectrolye thin films: Reversible cyclic voltammetry

Mario Tagliazucchi [a], Ernesto J. Calvo [a,*], Igal Szleifer [b]

[a] *INQUIMAE, DQIAyQF Facultad de Ciencias Exactas y Naturales, Universidad de Buenos Aires, 1428 Buenos Aires, Argentina*
[b] *Department of Biomedical Engineering, Northwestern University, 2145 Sheridan Road, Evanston, IL 60208, USA*

Received 28 November 2007; received in revised form 9 January 2008; accepted 17 January 2008
Available online 1 February 2008

Abstract

A molecular theory of chemically modified electrodes is applied to study redox polyelectroyte modified electrodes. The molecular approach explicitly includes the size, shape, charge distribution, and conformations of all of the molecular species in the system as well as the chemical equilibria (redox and acid-base) and intermolecular interactions. An osmium pyridine–bipyridine complex covalently bound to poly(allyl-amine) backbone (PAH-Os) adsorbed onto mercapto-propane sulfonate (MPS) thiolated gold electrode is described. The potential and electrolyte composition dependent redox and nonredox capacitance can be calculated with the molecular theory in very good agreement with voltammetric experiments under reversible conditions without the use of freely adjustable parameter. Unlike existing phenomenological models the theory links the electrochemical behavior with the structure of the polymer layer. The theory predicts a highly inhomogeneous distribution of acid-base and redox states that strongly couples with the spatial arrangement of the molecular species in the nanometric redox film.

Keywords: Molecular theory; Charge regulation; Modified electrode; Redox; Polyelectrolyte

1. Introduction

Brian Conway pioneered the molecular description of electrode reactions such as the hydrogen evolution reaction (HER). Also, in his well-known book on "Theory and Principles of Electrode Processes" there is a good description of non-ideal isotherms to describe molecular interactions in the adsorbate state [1]. Electrochemical experiments can be described quantitatively in terms of electron and mass transfer processes. A good example of this is the Marcus theory that provides a molecular description for simple outer sphere electron transfer reactions both in homogeneous solutions and at electrode surfaces [2]. More recently, a quantum mechanical description of electrochemical reactivity of quinones and their reactivity towards the oxygen reduction reaction (ORR) has made use of a theoretical approach of proton and electron transfer reactions [3,4].

In the last 30 years a considerable progress has been made in the development of "tailormade" electrode surfaces by chemical modification of electrodes with electroactive polymer films. A good description of electroactive polymer-modified electrodes can be found in the book edited by Lyon [5,6]. More recently the introduction of layer-by-layer self-assembly of polyelectrolyte multilayers [7–9] allowed a precision control of spatial molecular distribution in the nanoscale and fine regulation of the charge at the topmost layer. Several redox polyelectrolyte multilayers have been reported in chemically modified electrodes, i.e. poly(viologen) [10,11], poly(allylamine) with covalently attached ferrocene [12–19] or osmium pyridine-bi-pyridine redox centers [20–27], sulphonated poly(aniline) (SPAN) [28], etc. The use of these structures in biosensor platforms was introduced by Hodak et al. [13] with multilayers of glucose oxidase electrically connected to the underlying electrode by redox relays attached to the poly(allylamine) backbone [13]. A number of reports followed this development in the last 10 years using redox relays.

In spite of the extensive work on electrochemically active polymer-modified electrodes, much of the theoretical framework relies on phenomenological ideas rather than on a molecular description due to the molecular complexity of the problem [29–31].

* Corresponding author. Tel.: +54 1145763378; fax: +54 1145763341.
E-mail address: calvo@qi.fcen.uba.ar (E.J. Calvo).

0013-4686/$ – see front matter © 2008 Elsevier Ltd. All rights reserved.
doi:10.1016/j.electacta.2008.01.041

The first description of cyclic voltammetry of redox active species confined to electrode surfaces has been given by Gileadi and Srinivasan [32] who treated the adsorption pseudo-capacitance in Pt oxide or hydrogen adsorbed on platinum with an ideal Langmuir isotherm. The adsorption pseudo-capacitance due to non-charged and ionic species on electrodes has been described by Conway using Temkin or Frumkin non-ideal adsorption isotherms [1].

Considerable progress has been made since Laviron described mono [33,34] and multilayer [35] of redox films with lateral interactions which result in peak broadening, shape and width of voltammetric waves. Non-idealities in electroactive polymer films manifested as deviations in Nernst-type responses in plots of potential versus redox composition and peak broadening in linear potential sweep or cyclic voltammetry were also addressed by models that considered redox site interactions by Brown and Anson [36] and Albery et al. [37]. Chidsey and Murray [38] developed a microscopic model based on a cubic lattice with site interactions. These authors coined the term "redox capacity" for the stored electrons in a redox polymer and also incorporated interactions among the redox sites and the variation of counter ion activity as a function of the electrochemical potential. A chemical and mechanical description of polymer-modified electrodes was subsequently given by Bowden [39].

Charge and mass transport in polymer-modified electrodes has been considered in the models of Savéant and Andrieux [39,40] and also electron hopping by Blaunch et al. [40–43]. On the other hand, the effect of electrolyte concentration has been described by the Donnan exclusion model [20,44–47] or by the surface potential model [48]. Tagliazucchi et al. have recently described the pH dependence of redox active LbL multilayers using the Donnan potential analysis [49].

Smith and White [50] presented a model for an electrode coated with a monolayer of molecules bearing a weak acid headgroup. The model predicts a maximum in the capacitance–potential curves due to the dissociation of the acid at increasing metal/electrolyte potential difference. This prediction has been validated by cyclic voltammetry [51] and electrochemical impedance spectroscopy (EIS) [52,53] experiments for thiolated electrodes. This model has been extended to incorporate effects arising from the discreteness of charge [54–56]. It is interesting to note that only a recent treatment of polymer-modified electrodes has used a statistical description of polymer chains, based on the Flory theories for polymer free energy of mixing and elastic deformation [57–59].

Despite the descriptive value of all these previous models they provide only a partial depiction of the electrochemical process and do not include specific molecular characteristics of the polymer film, such as conformational degrees of freedom of polymer chains, the shape and size of the molecules, the local activity coefficients of the electroactive species, the properties of underlying substrates (i.e. thiol layers) and the coupling of acid base and redox equilibria.

We have recently presented a molecular theory based on minimization of the free energy functional of the system and obtained the molecular organization of the film as a function of the bulk pH, salt concentration, and applied electrode potential [60]. The free energy explicitly includes the intra and intermolecular interactions, the distance dependent acid base equilibrium of the ionizable group of the weak polyelectrolyte, the distant dependent redox equilibria of the redox electrochemical active sites with the metal together with the size, shape, charge distribution and different conformations of all the different molecular species. Together with the structural features the theory enables the determination of the thermodynamic properties of the film as well as the calculation of the current–potential curves that can be directly compared with experimental observations. Moreover, the understanding of the molecular organization and the predictions of the equilibrium electrochemical behavior of the modified electrode provides for the fundamental molecular understanding of the relationship between layer structure and electrochemical response [60].

As a first step of a molecular theory for chemically modified electrodes with redox active self-assembled polyelectrolye layers we begin by describing the redox pseudo-capacitance of a reversible one-electron redox couple confined to the electrode surface. The non-redox and redox capacitances can be obtained from the excess surface charge in the metal and the population of redox states in the film at a given electrode potential, respectively [1]:

$$C_{\text{non-redox}} = \frac{\partial \sigma_{\text{M}}}{\partial E_{\text{eq}}} \tag{1}$$

and [38],

$$C_{\text{redox}} = F\frac{\partial \Gamma_{\text{o}}}{\partial E_{\text{eq}}} \tag{2}$$

With Γ_{o}, the total surface concentration of the oxidized species, F is the Faraday constant, σ_{M} the surface charge per unit area at the metal and the derivatives are taken with respect to the reversible electrode potential. The molecular theory allows to theoretically determine both the surface concentration of oxidized sites and the surface charge as a function of the applied potential from which the capacitance can be directly calculated, provided the total surface redox charge is known.

In this paper we present predictions of the molecular theory and direct comparisons with experimental results for low scan voltammetry. Furthermore, we compare with previously developed (phenomenological) models to account for the current–potential curves under reversible conditions, the peak potential and peak width and their dependence on the concentration of electrolyte and pH. We will show that while the phenomenological models require fitting parameters to compare with the experimental observations, the molecular theory provides for an understanding of the source of these parameters as well as a detailed description of the distribution of all the molecular species and electrical potential in the normal direction to the surface. Thus, while in general the molecular theory is computationally more demanding than the phenomenological models, its predictive power is based on the knowledge of the molecular species composing the system and the value of the experimental controlled variables, such as bulk pH, ionic strength and applied potential. In this way we obtain a detailed description of the rela-

tionship between the molecular organization within the film, its variation upon changes in the external controlled variables and the electrochemical response of the modified electrode.

2. Molecular theory and model

The molecular theory for polymer-modified electrodes allows us to determine the structure and equilibrium electrochemistry [60] of a polymer-modified electrode from a first principle calculation (within the given molecular model and approximations). An illustrative chart showing the different steps involved in the formulation and solving of the theory is presented in Fig. 1A. In Fig. 1B we show a cartoon of our model system, a single layer of PAH-Os adsorbed on a gold electrode thiolated with MPS.

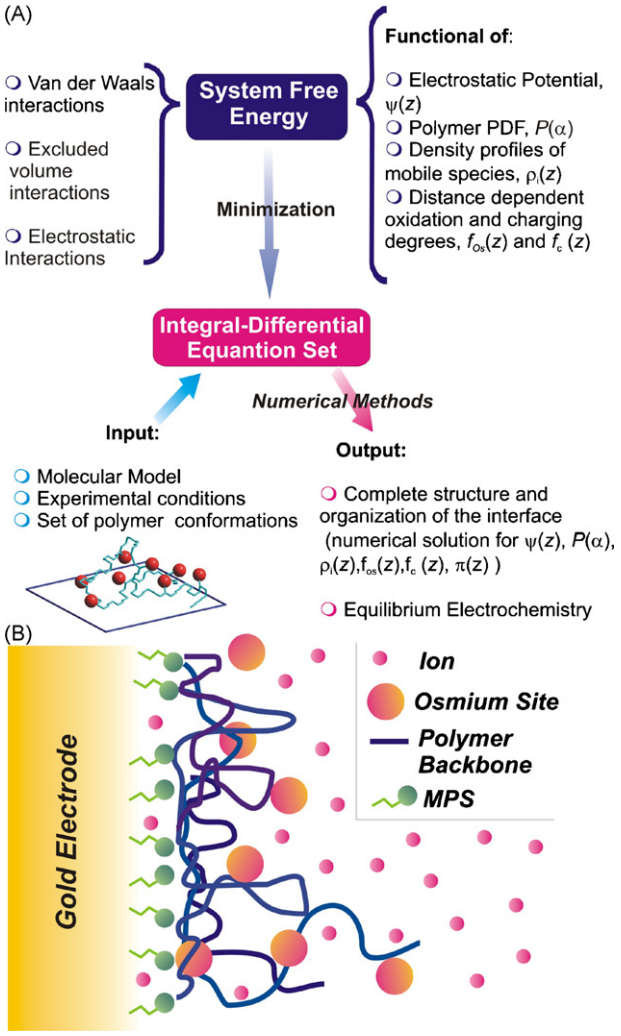

Fig. 1. (A) Flow chart showing the steps involved in writing down and solving the molecular theory. (B) Cartoon of the Au/MPS/PAH-Os/solution interface. The poly(allylamine) backbone and the pyridine–bipyridine osmium complexes of PAH-Os are represented by blue solid lines and big spheres, respectively. The allylamine units in the polymer backbone can be either protonated (charge +1) or deprotonated (neutral) and the osmium complexes can be in an oxidized Os(III) (charge +2) or in a reduced Os(II) (charge +1) state. MPS molecules form a permeable layer on the gold. The headgroup in MPS can exist as a negatively charged sulfonate or as a neutral sulfonic acid. The electrode is immersed in an aqueous electrolyte solution.

This redox polyelectrolyte ultrathin film is the basis of an all-integrated "wired" glucose oxidase (GOx) biosensor. The chains of the redox polyelectrolyte PAH-Os are composed of a polymer backbone (poly-allylamine) and the tethered osmium sites (osmium pyridine–bipyridine complex). They are adsorbed on a gold electrode thiolated with mercapto-propansulfonate (MPS). The whole system is immersed in an electrolyte solution containing salt ions, protons and hydroxyl groups. The concentrations of these mobile species in the bulk are determined by the ionic strength and pH of the testing solution. The sulfonate groups in the thiol and the amino groups in the polymer backbone are protonable groups and therefore can exist either in a basic or in an acid form The osmium sites are redox active and its oxidized Os(III) and reduced Os(II) forms can be interconverted by exchanging electrons with the underlying metal. This process depends on the potential at the electrode and the local activity of the redox sites.

In order to formulate the theory [60] we start by writing down the free energy of the system as a functional of the densities of all the mobile species in the system (solvent, protons, hydroxyl ions and salt ions), the probabilities of all possible conformations for polymer chains, the electrostatic potential and the degrees of protonation and oxidation for acid–base and redox groups, respectively. All these quantities depend in principle on the three dimensions of the problem (i.e. are functions of x, y and z), however, we consider only inhomogeneities in the direction normal to the electrode (z) and use a mean-field approximation for the planes parallel to the gold surface. For simplicity we neglect the roughness of the substrate and therefore the electrode is located in the xy plane at $z=0$. We write the free energy functional of the system as:

$$\begin{aligned} F = &-\mathrm{TS}_{\mathrm{w,mix}} - \mathrm{TS}_{\mathrm{A,mix}} - \mathrm{TS}_{\mathrm{C,mix}} - \mathrm{TS}_{\mathrm{H^+,mix}} - \mathrm{TS}_{\mathrm{OH^-,mix}} \\ &- \mathrm{TS}_{\mathrm{pol}} - \mathrm{TS}_{\mathrm{MPS}} - \mathrm{TS}_{\mathrm{NH_2/NH_3^+}} - \mathrm{TS}_{\mathrm{SO_3^-/HSO_3}} \\ &- \mathrm{TS}_{\mathrm{Os(III)/Os(II)}} + F_{\mathrm{e^-}} + F_{\mathrm{vdW}} + F_{\mathrm{Elec}} + F_{\mathrm{P\text{-}S}} + F_0 \\ &+ F_{\mu_{\mathrm{C}}} + F_{\mu_{\mathrm{A}}} \end{aligned} \quad (3)$$

The terms in Eq. (3) describe different contributions to the free energy of the system. Table 1 includes a brief description of each of them and their mathematical expressions. A glossary describing the symbols is included at the end of the paper. The reader is referred to our previous publication [60] for an in depth analysis of each contribution. The minimization of the free energy is carried out considering two constraints: the global electroneutrality constrain and the packing constraint, whose expressions are given in Table 1. The packing constraint is introduced in order to account for repulsive interactions, which are modeled as excluded volume interactions [61].

Upon minimization of the free energy, we obtain expressions for the density profile of mobile ions and solvent molecules, $\rho_i(z)$; the probability distribution function for the polymer, $P(\alpha)$; the protonation fraction of amines and sulfonates, $f_c(z)$ and $f_{c,\mathrm{MPS}}(z)$; the osmium oxidation degree, $f_{\mathrm{Os}}(z)$ and $\psi(z)$ the distance dependent electrostatic potential. These expressions are expressed in terms of the relevant interaction fields as expressed next.

Table 1
Contributions to the system free energy, Eq. (3)

Term in equation	Contribution to the free energy	Expression
Terms of the free energy		
$S_{i,\mathrm{mix}}/Ak_\mathrm{B}$	Translational entropy of mobile ions and water molecules (i: A, C, OH^-, H^+, w)	$-\int \rho_i(z)[\ln(\rho_i(z)v_\mathrm{w})-1]\,\mathrm{d}z$
$S_\mathrm{pol}/Ak_\mathrm{B}$	Conformational entropies of polymer chains	$-\frac{N_\mathrm{P}}{A}\left[\sum_\alpha P_\mathrm{P}(\alpha)\ln\ P_\mathrm{P}(\alpha)\right]$
$S_\mathrm{MPS}/Ak_\mathrm{B}$	Conformational entropies of thiol molecules	$-\frac{N_\mathrm{MPS}}{A}\left[\sum_\gamma P_\mathrm{MPS}(\gamma)\ln\ P_\mathrm{MPS}(\gamma)\right]$
$S_{\mathrm{NH_2/NH_3^+}}/Ak_\mathrm{B}$	Amine acid–base equilibrium mixing entropy	$-\int \langle n_\mathrm{P}(z)\rangle\,[f_\mathrm{c}(z)\ln(f_\mathrm{c}(z))+(1-f_\mathrm{c}(z))\ln(1-f_\mathrm{c}(z))]\,\mathrm{d}z$
$S_{\mathrm{SO_3^-/HSO_3}}/Ak_\mathrm{B}$	Sulfonate acid–base equilibrium mixing entropy	$-\int \langle n_\mathrm{MPS}(z)\rangle\,[f_\mathrm{c,MPS}(z)\ln(f_\mathrm{c,MPS}(z))+(1-f_\mathrm{c,MPS}(z))\ln(1-f_\mathrm{c,MPS}(z))]\,\mathrm{d}z$
$S_\mathrm{Os(III)/Os(II)}/Ak_\mathrm{B}$	Osmium redox equilibrium mixing entropy	$-\int \langle n_\mathrm{Os}(z)\rangle\,[f_\mathrm{Os}(z)\ln(f_\mathrm{Os}(z))+(1-f_\mathrm{Os}(z))\ln(1-f_\mathrm{Os}(z))]\,\mathrm{d}z$
$\beta F_{e^-}/A$	Electrical work to achieve the final redox state of the system from electrons in the environment	$E_\mathrm{eq}^\mathrm{abs}\beta\lvert e\rvert\int\langle n_\mathrm{Os}(z)\rangle\,[1-f_\mathrm{Os}(z)]\,\mathrm{d}z$
$\beta F_\mathrm{vdw}/A$	van der Waals (vdW) polymer-polymer interactions	$\iint\frac{\beta\chi(\lvert z-z'\rvert)}{2}[\langle\phi_\mathrm{Os}(z)\rangle+\langle\phi_\mathrm{P}(z)\rangle][\langle\phi_\mathrm{Os}(z')\rangle+\langle\phi_\mathrm{P}(z')\rangle]\,\mathrm{d}z\,\mathrm{d}z'$
$\beta F_\mathrm{Elec}/A$	Coulombic Interactions	$\beta\int[\langle\rho_Q(z)\rangle\,\psi(z)-(1/2)\varepsilon(z)(\nabla_z\psi(z))^2]\,\mathrm{d}z$
$\beta F_\mathrm{P-S}/A$	van der Waals (vdW) polymer–surface interactions	$\frac{N_\mathrm{P}}{A}\left[\sum_\alpha P_\mathrm{P}(\alpha)\beta U_\mathrm{PS}(\alpha)\right]$
$\beta F_0/A$	Standard chemical potentials (μ_i^0) for those species participating in chemical equilibria	$\int\langle n_\mathrm{P}(z)\rangle\,(f_\mathrm{c}(z)\beta\mu^0_{\mathrm{NH_3^+}}+(1-f_\mathrm{c}(z)\beta\mu^0_{\mathrm{NH_2^+}})\,\mathrm{d}z$ $+\int\langle n_\mathrm{MPS}(z)\rangle\,(f_\mathrm{c,MPS}(z)\beta\mu^0_{\mathrm{SO_3^-}}+(1-f_\mathrm{c,MPS}(z)\beta\mu^0_{\mathrm{HSO_3}})\,\mathrm{d}z$ $+\int\langle n_\mathrm{Os}(z)\rangle\,(f_\mathrm{Os}(z)\beta\mu^0_{\mathrm{Os(III)}}+(1-f_\mathrm{Os}(z)\beta\mu^0_{\mathrm{Os(II)}})\,\mathrm{d}z$ $+\int\mu^0_{\mathrm{H^+}}\rho_{\mathrm{H^+}}(z)\,\mathrm{d}z+\int\mu^0_{\mathrm{OH^-}}\rho_{\mathrm{OH^-}}(z)\,\mathrm{d}z$
$\beta F_{\mu_i}/A$	Chemical potentials of anions (i = A) and cations (i = C)	$-\beta\mu_i\int\rho_i(z)\,\mathrm{d}z$

Constraint	Expression
Minimization constraints	
Global electroneutrality	$\int\langle\rho_Q(z)\rangle\,\mathrm{d}z+\sigma_\mathrm{M}=0$
Packing constraint	$\sum_i\langle\phi_i(z)\rangle=1$

The distance dependent densities for water molecules, $\rho_\mathrm{w}(z)$, is given by

$$\rho_\mathrm{w}(z)v_\mathrm{w}=\rho_\mathrm{w}^\mathrm{bulk}v_\mathrm{w}\exp(-v_\mathrm{w}\beta[\pi(z)-\pi^\mathrm{bulk}]) \quad (4)$$

where $\beta=1/k_\mathrm{B}T$ is the inverse absolute temperature, $\pi(z)$ is a Lagrange multiplier associated with the packing constraint, which can be regarded as a lateral osmotic pressure [61] and v_w is the molecular volume of the solvent. An expression similar to Eq. (4) describes the local density of mobile ions, $\rho_i(z)$, ($i=H^+$, OH^-, C, A for proton, hydroxyls, cations and anions, respectively):

$$\rho_i(z)v_\mathrm{w}=\rho_i^\mathrm{bulk}v_\mathrm{w}\exp(-\nu_i\beta[\pi(z)-\pi^\mathrm{bulk}]-q_i\beta[\psi(z)-\psi^\mathrm{bulk}]) \quad (5)$$

where $v_i(z)$ and q_i are the molecular volume and charge of the species i, respectively. $\pi(z)$ and $\psi(z)$ represent the repulsive and electrostatic interaction fields at z. These fields are determined from the average distribution of all the different species across the film. Therefore, they couple the interactions between molecules in different zones of the interface, i.e. they are highly non-local [62].

We assume that the polymer chains are adsorbed to the surface at fixed total surface density. On the other hand, the segment density profile is unknown and should be determined by the theory considering the probability of each conformation and its segment distribution. While the different allowed conformations are inputs, the relative population of each one is an output obtained from the theory and it varies with the experimental controlled variables (e.g. bulk pH, solution ionic strength and applied potential). For a chain in conformation α we have

$$P_\mathrm{P}(\alpha)=\frac{1}{\xi}\exp\{-\int n_\mathrm{P}(z,\alpha)[\ln(f_\mathrm{c}(z))+q_{\mathrm{NH_3^+}}\beta\psi(z)]\,\mathrm{d}z-\int n_\mathrm{Os}(z,\alpha)[q_\mathrm{Os(II)}\beta\psi(z)+\ln(1-f_\mathrm{Os}(z))]\,\mathrm{d}z-\beta U_\mathrm{PS}(\alpha)-\int[v_\mathrm{P}(z,\alpha)+v_\mathrm{Os}(z,\alpha)][\beta\pi(z)+\int\beta\chi(\lvert z-z'\rvert)(\langle\phi_\mathrm{P}(z')\rangle+\langle\phi_\mathrm{Os}(z')\rangle)\,\mathrm{d}z']\,\mathrm{d}z\} \quad (6)$$

where $n_i(z,\alpha)$ and $v_i(z,\alpha)$ are the number and volume of allylamine segments or osmium sites (i = P, Os, respectively) that a PAH-Os chain in conformation α has at z, $U_{PS}(\alpha)$ is the polymer–surface interaction energy for a chain in conformation α, $\chi(|z-z'|)$ is a distance dependent van der Waals interaction parameter [63], ξ is a normalization constant and $\langle\phi_i(z)\rangle$ is the average volume fraction of species i at z. In this equation the probability of having a chain in a given conformation depends on the interaction fields and therefore the distribution of polymer segments and osmium sites is coupled to the distribution of the other species. Eq. (6) also contains contributions from the strength of van der Waals forces and the fraction of oxidized osmium sites and protonated amino groups. These fractions are self-consistently determined from the equations describing chemical equilibria, which are also given by the theory from the minimization of the free energy with respect to $f_c(z)$ and $f_{Os}(z)$.

For the acid–base equilibrium of the allylamines the equilibrium constant is given by:

$$K_b^0 = \exp[-\beta\Delta G_c^0] = \frac{\rho_{OH^-}(z) f_c(z)}{1 - f_c(z)} \exp(v_{OH^-}\beta[\pi(z) - \pi^{bulk}]) \quad (7)$$

In this expression, K_b^0 is the thermodynamic equilibrium constant, which can be multiplied by N_A/ρ_w^{bulk} (with N_A equal to Avogadro's number) to obtain the commonly used equilibrium constants based on the molar bulk concentration reference state. In Eq. (7), $\Delta G_c^0 = \mu_{OH^-}^0 + \mu_{NH_3^+}^0 - \mu_{NH_2}^0$ is the standard free energy change for the reaction:

$$P\text{-}NH_2 + H_2O \rightleftarrows P\text{-}NH_3^+ + OH^- \quad (8)$$

It is important to note that the exponential term in the right hand side of Eq. (7) is an activity coefficient term. This term depends on the interaction field $\psi(z)$, which is non-local and therefore it couples with all the interactions and chemical equilibria in all regions of the film.

We consider also the acid–base equilibrium given by the protonation of the sulfonates in the thiol:

$$Au\text{-}S(CH_2)_3SO_3H + H_2O \rightleftarrows Au\text{-}S(CH_2)_3SO_3^- + H_3^+O \quad (9)$$

which is determined by the expression

$$K_{\alpha,MPS}^0 = \exp[-\beta\Delta G_{c,MPS}^0] = \frac{\rho_{H^+}(z) f_{c,MPS}(z)}{1 - f_{c,MPS}(z)} \exp(v_{H^+}\beta[\pi(z) - \pi^{bulk}]) \quad (10)$$

$f_{c,MPS}(z)$ is the fraction of sulfonate groups that are charged at z and $\Delta G_c^0 = \mu_{H^+}^0 + \mu_{SO_3^-}^0 - \mu_{HSO_3}^0$ is the standard free energy change for reaction (9).

In addition to acid–base equilibrium, the system under study has osmium sites which are in redox equilibrium with the metal in their +2 and +3 states:

$$P\text{-}Os(III)^{+2} + e^-(Au) \rightleftharpoons P\text{-}Os(II)^+ \quad (11)$$

The theory provides for a generalized Nernst equation for this redox couple

$$E_{eq}^{abs} = E_{Os(III)/Os(II)}^{0,abs} + \frac{RT}{F}\ln\left(\frac{f_{Os}(z)}{1 - f_{Os}(z)}\right) + \frac{(q_{ox} - q_{red})}{|e|}\psi(z) \quad (12)$$

where E_{eq}^{abs} is the electrode potential and $E_{Os(II)/Os(III)}^{0,abs}$ is the standard thermodynamic redox potential in the absolute scale. It is important to emphasize that while Eq. (12) seems to be local, the non-local effect are hidden in the fact that both $\psi(z)$ and $f_{Os}(z)$ are strongly coupled with the other interaction fields at all distances from the surfaces. Namely, changes in the value at one distance from the surface, results in changes at all z's.

The absolute potential scale is used in the theory because we need to deal with the outer electrostatic potential, $\psi(z)$, which is zero at the infinite vacuum. The electrode potentials in Eq. (12) can be converted into the experimental potential scale (Ag/AgCl) using the potential of the Ag/AgCl electrode in the absolute scale taken from the work of Trasatti [64,65]. The Ag/AgCl potential scale will be used hereafter to present both experimental and theoretical results. Note also that the Nernst equation depends not on the concentrations but on the activities and that the activity coefficients are given by the last term of the right-hand side of Eq. (12).

The extremum of the free energy with respect to $\psi(z)$ yields the generalized Poisson–Boltzmann (GPB) equation for electrostatics

$$\nabla(\varepsilon(z)\nabla\psi(z)) = -\langle\rho_Q(z)\rangle \quad (13)$$

where $\varepsilon(z)$ is the local dielectric constant and $\langle\rho_Q(z)\rangle$ is the total average charge at distance z from the metal electrode. It is important to emphasize that Eq. (13) includes all the interaction present in the system. Namely, the average charge at z is determine using Eqs. (4)–(7), (10), (12) and (13) and therefore the GPB accounts for the full potential of mean-force between the different species. This is one more example of the non-linear and complex coupling between all the interactions as manifested in Eqs. (4)–(7), (10), (12) and (13).

The boundary conditions for the GPB equation are the electrostatic potential in the bulk which we set to zero and on the metal which is determined from the electrode potential in the absolute potential scale by:

$$\psi^M = E_{eq}^{abs} - \frac{\Phi_{e^-}^M}{|e|} \quad (14)$$

where $\Phi_{e^-}^M$ is the work function of the metal ($\phi_{Au} = -4.7$ eV) [64,65] and $|e|$ is the elementary electrical charge.

The set of integral-differential equations given by Eqs. (4)–(7), (10), (12) and (13) and the packing constraint in Table 1 is solved numerically. The input necessary to solve the equations includes the molecular information of the species in the system, i.e. their size, charge, charge distribution, and conformations; the strength of the interactions, i.e. the van der Waals coefficients and the standard free energy for the appropriate acid–base

and redox reactions. In addition to the molecular model, the equations require as an input the experimental conditions, i.e. bulk salt concentration, pH, electrode potential and surface coverage of polymer chains and thiol molecules. The numerical solution of the equations resulting from the minimization of the free energy provides as output the following functions: $\psi(z)$, $\rho_i(z)$, $\pi(z)$, $P(\alpha)$, $f_c(z)$, $f_{c,MPS}(z)$ and $f_{Os}(z)$. From the knowledge of these functions we can calculate any desired average conformational and thermodynamic property of the modified electrode. For example, equilibrium electrochemistry is determined by solving the theory for increasing electrode potentials and calculating the redox and non-redox contributions to the electrode capacitance by rewriting Eqs. (1) and (2) as:

$$C_{\text{redox}} = F\frac{\partial \Gamma_{\text{Os(III)}}}{\partial E_{\text{eq}}^{\text{abs}}} = F\frac{\partial \int \langle N_{\text{Os}}(z)\rangle\, f_{\text{Os}}(z)\,\mathrm{d}z}{\partial E_{\text{eq}}^{\text{abs}}} \quad (15)$$

$$C_{\text{non-redox}} = \frac{\partial \sigma_{\text{M}}}{\partial E_{\text{eq}}^{\text{abs}}} = \frac{\partial(-\varepsilon(0)(\partial\psi/\partial z)(0))}{\partial E_{\text{eq}}^{\text{abs}}} \quad (16)$$

where $\Gamma_{\text{Os(III)}}$ is the surface concentration of Os(III) and σ_{M} the charge in the metal. The total capacitance is given by the sum of C_{redox} and $C_{\text{non-redox}}$.

We will briefly describe the molecular model used in the theory. Table 2 contains the charge, volume and equilibrium constants of the participating species as well as the surface densities for grafted species. The MPS layer is considered to form a permeable layer of thickness 0.5 nm, with a surface coverage obtained from the literature [66] and an effective dielectric constant of 3.8 calculated with the Maxwell–Garnet formula [67,60]. We allow mobile ions to penetrate this layer, but not polymer chains and neglect any variation of the dielectric constant and thiol film thickness due to ion population changes. The surface density of PAH-Os chains, determining the surface coverage of allylamine units and osmium sites, was obtained from the integrated redox peak and the osmium to segment ratio (1:13 from XPS measurements) [49]. Chains were constrained to have at least one segment in contact with the thiol layer in order to avoid desorption. Each polymer chain was modeled as a linear backbone of 130 segments bearing 10 osmium sites and polymer conformations were generated using a modified Rosenbluth–Rosenbluth algorithm as described in Ref. [60] in order to optimize sampling. The interaction strengths between polymer segments and osmium sites with the thiolated surface is −1.0 kT and −2.0 kT, respectively and polymer–polymer interactions are chosen to give an effective temperature for the solvent of 0.75θ [68] which corresponds to poor solvent conditions. The standard redox potential of the Os(III)/Os(II) redox couple (i.e. the value in the absence of interactions) can obtained from the cyclic voltammetry of the soluble complex and the pK_a of allylamine and sulfonate are estimated from bibliographic values for similar molecules [69].

3. Experimental results and molecular theory predictions

Fig. 2 presents slow scan rate (25 mV s^{-1}) current–potential curves for Au/MPS/PAH-Os modified electrodes in 4 mM and 1.2 M $NaNO_3$ and 1 mM HNO_3 solutions of pH 3 (circles), respectively. The redox charge is constant at low scan rate ($\leq$0.1 V s^{-1}) and the small peak separation (c.a. less than 10 mV) corresponds to a reversible electron transfer process between electronic states at the gold electrode and the Os(III)/Os(II) redox couple in the polyelectrolyte film.

Fig. 3 shows slow scan rate redox current–potential curves for the same system in electrolyte solutions of different pH (pHs 4 and 9, respectively) and 4 mM $NaNO_3$. At the lowest electrolyte concentration, 4 mM, the peak potential position exhibits the maximum change, whereas at higher concentration the effect is screened by the ions.

The experiment shows that the peak position and full peak width at half-height (FWHH) for these surface redox waves is dependent on the concentration of electrolyte and pH.

In both figures we have also presented the capacitance–potential curve predicted by the molecular theory (Eqs. (15) and (16)) which captures all the features: peak shape and width and

Table 2
Molecular model for Gold/MPS/PAH-Os/Electrolyte system

Specie	Electrostatic charge q_i	Molecular volume, v_i (Å^3)
Solution species		
Water	0	30
Cation	+1	33.5
Anion	−1	33.5
Proton	+1	30
Hydroxyl ions	−1	30

Specie	Electrostatic charge, q_i	Molecular (segment) volume, v_i (Å^3)	Equilibrium constant	Surface density (mol cm^{-2})
Grafted species				
Polymer segment (allylamine)	+1 (NH_3^+) 0 (NH_2)	113	pK_b = 11.0	3.5×10^{-10}
Thiol molecule	−1 (SO_3^-) 0 (HSO_3)	580	pK_a = 0.0	4.6×10^{-10}
Redox site (osmium complex)	+2 (Os^{III}) +1 (Os^{II})	1770	$E^0_{\text{Os(III)/Os(II)}} = 0.265$ V (vs. Ag/AgCl)	2.65×10^{-11}

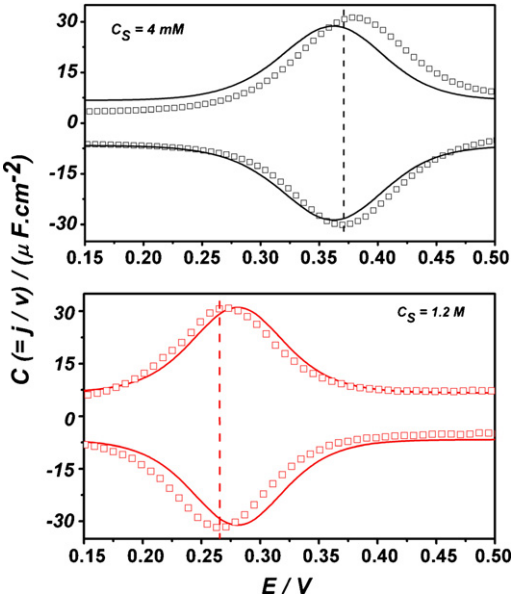

Fig. 2. Comparison of experimental (squares, $v = 0.025$ V/s) and theoretical (solid lines) current–potential plots measured for a Au/MPS/PAH-Os electrode in solutions of different ionic strength and 1 mM HNO_3 (pH 3).

peak potential and their dependence with electrolyte concentration and pH. It should be emphasized that the theory predicts the experimental result without any adjustable parameter. The only information provided is the bulk pH, solution ionic strength and the total amount of redox polymer that is experimentally obtained from integration of the redox charge. Namely, the solid lines in Figs. 2 and 3 have been calculated and are not fits to the experimental data.

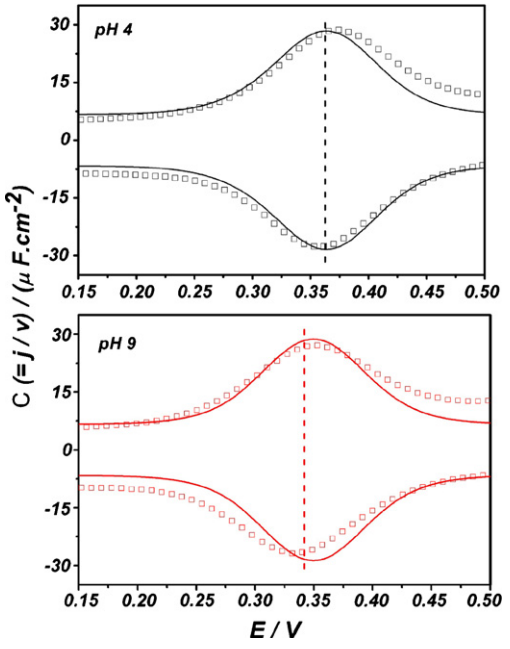

Fig. 3. Comparison of experimental (squares, $v = 0.025$ V/s) and theoretical (solid lines) current–potential plots measured for a Au/MPS/PAH-Os electrode in solutions of different pH (prepared from 1 mM NaOH and HNO_3 solutions containing 4 mM $NaNO_3$).

The experimental observations can also be analyzed with different existing models which are valid under restricted conditions. For instance, Laviron [33] has described a model for the redox capacitance curve shape, the non-ideal behavior expressed in the peak broadening can be accounted for by the models of Laviron, Anson [36] and Albery et al. [37] and Bowden [39]. The peak shift with electrolyte concentration can be described by the Donnan model [20,44,49] while the pH dependence can be described by the scheme of squares of Laviron [35] and the Smith and White formalism [50]. In all these treatments the experimental data are described in terms of adjustable parameters obtained by fitting the experimental data: examples of these adjustable parameters are the interaction parameters for a non-ideal isotherm, the activity coefficients or distribution width of redox potential population, the fixed charge in the polymer for the Donnan exclusion model, the activity coefficients or distribution width of the pK_a values, etc. Moreover, the models that have been employed so far have no predictive capability and are only applicable under restricted experimental conditions. It should also be noted that these models do not provide information on the structure of the interface.

The molecular theory, on the other hand, employs no free adjustable parameters, and once the correct molecular description is employed it solves for the distribution of all polymer and mobile species and the electrostatic potential profile. Thus, the non-redox and the redox components of the electrode capacitance are given in terms of the molecular theory output: the electrostatic potential ($\psi(z)$), the distribution density of redox sites ($\langle n_{Os}(z)\rangle$) and the fraction of oxidized osmium sites ($f_{Os}(z)$) in the film as a function of the normal distance to the electrode.

The capacitance– potential curves calculated with the molecular theory in Fig. 2 for two different salt concentrations (solid lines) are in very good agreement with the experimental results, both for the peak position (E_{peak}) and peak full width at half-height (FWHH). The shift of the peak potential with electrolyte concentration is depicted in Fig. 4 for the entire range of ionic strength under investigation.

The dependence of peak potential with ionic strength can be analyzed with the Donnan model [44] for thick membranes carrying a fix charge in equilibrium with an electrolyte or by the surface potential model [48] for a thin membrane in equilibrium with an electrolyte solution. For a membrane of thickness larger than the Debye length, the fix charges in the film set a Donnan potential that excludes ions of the same charge in the adjacent electrolyte. The shift in the apparent redox potential is equal to the interfacial electrical potential that arises due to the different ionic composition inside the film and in the electrolyte:

$$E_{1/2}^{app} = E^0_{Os(III)/Os(II)} + \Delta\phi_{Donman} \quad (17)$$

where $E^0_{Os(III)/Os(II)}$ is the redox potential of the Os(II)/Os(III) complex in the absence of electrostatic work terms due to the charged polymer film, i.e., in solution, and $\Delta\phi_D$ is the interfacial Donnan potential [44]:

$$\Delta\phi_{Donman} = \frac{RT}{F} \ln\left[\frac{c_F + (c_F^2 + 4c_S^2)^{1/2}}{2C_S}\right] \quad (18)$$

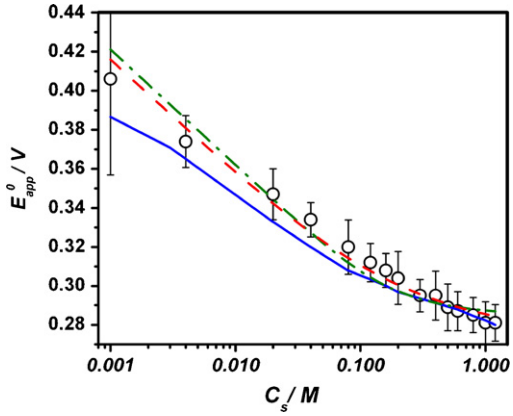

Fig. 4. Plots of peak potential position vs. salt concentration in the bulk solution determined from the experimental ($v = 0.025$ V/s, circles) and theoretical redox waves predicted by the molecular theory (solid line) for HNO_3 1 mM (pH 3). The experimental data presented is an average from the oxidation and reduction peaks obtained from three different sets of cyclic voltammetry experiments. The error bars indicate three standards deviations from the average. The best-fit curves of experimental data with the Donnan partition model (dot-dashed line, Eq. (18)) and the Gouy-Chapman theory (dashed line, Eq. (19)) are also shown.

where C_S represents, for a 1:1 electrolyte the ionic concentration in the external solution and C_F, concentration of fix charged sites in the polymer which can be positive or negative for films bearing fixed positive or negative fixed ionic charges. In the present case both the thiol and polymer layer contribute to the fix charge. Since the Donnan model is a two-phase model the interfacial potential distribution is neglected.

On the other hand, when all the charge is confined at the electrode surface (thickness $\ll$ Debye length), the surface potential with respect to the solution ϕ_s is related to the surface charge density, σ_M; ε_r the relative permittivity and ε_0 the permittivity of vacuum [48]:

$$\phi_S = \frac{2RT}{F} \operatorname{arcsin} h \left[\frac{\sigma_M}{(8c_s\varepsilon_r\varepsilon_o kT)^{1/2}} \right] \quad (19)$$

Fig. 4 shows the best-fit curves for a Donnan model with $C_F = 0.20$ M and $E^0_{Os(III)/Os(II)} = 0.28$ V (dot-dashed curve) and for a surface potential model (Gouy-Champman) with $\sigma_S = 3.02\ \mu C\,cm^{-2}$ and $E^0_{Os(II)/Os(III)} = 0.27$ V (dashed curve), respectively.

None of these limiting models is strictly applicable to the experimental data since the ellipsometric film thickness, 1.5 nm, lies in between the values of the Debye length for $C_S = 1$ mM (9.6 nm) and for $C_S = 1$ M (0.3 nm). However, within the Donnan model we can estimate the surface charge with the ellipsometric thickness and $C_F = 0.20$ M, which yields $\sigma_S = 2.89\ \mu C\,cm^{-2}$. This results is consistent with the value obtained from the Gouy-Champman theory. Furthermore, it is appealing to estimate the surface charge as the sum of the surface charges of the different species at the interface: integration of low scan rate cyclic voltammetry yields $2.56\ \mu C\,cm^{-2}$ for the osmium sites; from the molecular structure we obtain $33.3\ \mu C\,cm^{-2}$ for the NH_3^+ (1:13 osmium to PAH segment ratio); and from thiol monolayer covergage $-43.0\ \mu C\,cm^{-2}$ [66]. A total negative net charge density of $-7.14\ \mu C\,cm^{-2}$ results, which differs with the fitted value of $\sigma_S = 3.02\ \mu C\,cm^{-2}$. While this calculation is independent on the molecular model of the system, the molecular theory allow us to examine this situation and provides a quantitative explanation for this apparent contradition. The theory predicts that in order to minimize the electrostatic repulsion in the thiol layer, sulfonate groups become partly protonated [70]. We found that, due to charge regulation, the fraction of charged sulfonate groups (at pH 3, 4 mM electrolyte and an oxidation fraction of 0.5) is 0.76 and therefore the total charge density at the interfacial region is $3.18\ \mu C\,cm^{-2}$, very close to the fited value. In a previus work [70], we have shown that the high surface charge of the thiol layer also induces the charge regulation of the adsorbed polyelectrolyte. As a consequence, the allylamines on a thiolated surface become more easily protonated than on a neutral substrate and therefore the aparent pK_a is increased.

The pH dependence of peak potential is depicted in Fig. 5, showing that the theory successfully predicts both the dependence of peak potential with the ionic strength and pH. The pH dependence of the peak position for pH-independent couples is caused by intermolecular interactions and has been much less studied than the dependence on salt concentration. In the present case the Os(III)/Os(II) redox couple is pH-independent but the film bears protonable positively charged amino groups, and therefore it is appealing to make an analogy with a $1e^-/1H^+$ system, which can be modeled by a scheme of squares (see Fig. 6) for the reactions that exchange both electrons and protons. Fig. 5 shows two well defined regions: below pH 10, the number of positive charges in the film is independent of pH and the reaction involves only the protonated polymer. Therefore the peak potential is almost constant in that region. In the range $10 < pH < 12$, the deprotonation of the amino groups in the film leads to a decrease of the peak potential at increasing electrolyte pH. From the analogy with a $1e^-/1H+$ system, we expect that at $pH > 12$, most of the amino groups in the film should become deprotonated and the peak position must be again pH-independent. The square scheme in Fig. 6 shows that the electron transfer reaction can proceed through protonated or deprotonated polymer. While it is possible to use in principle the $1e^-/1H+$ model to fit peak position vs. pH experimental data (similar to that in Fig. 5), we have shown that the agreement between fitting parameters and the predictions of the theory is rather poor [70] and therefore the analogy with $1e^-/1H+$ model

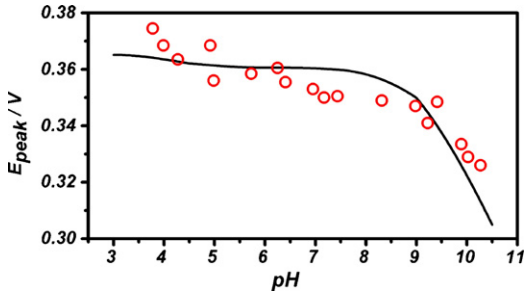

Fig. 5. Comparison between theoretical (solid line) and experimental ($v = 0.025$ V/s, circles) voltammetric peak potential for electrolyte solutions of different pH (prepared from 1 mM NaOH and HNO_3 solutions containing 4 mM $NaNO_3$).

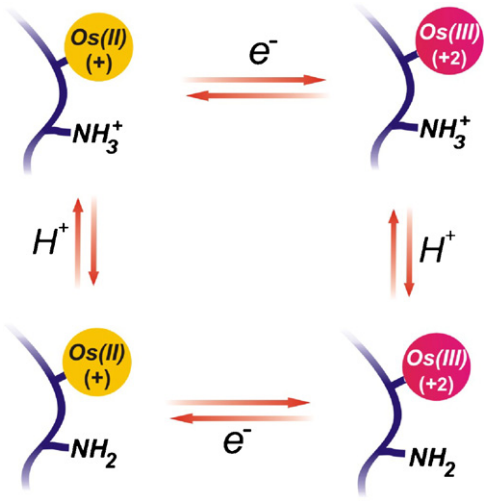

Fig. 6. Square scheme for PAH-Os film showing the analogy with a 1e⁻/1H+ redox couple.

cannot be extended beyond the qualitative description analyzed above.

Fig. 7 shows the analysis of the redox capacitance depicted in Fig. 2 in the positive potential scan. The figure clearly shows the widening of the peak recorded in $C_S = 1$ mM. The results are analyzed with the model of Brown and Anson [36] which considers the surface activity coefficients to explain the non-ideal electrochemical behavior. The logarithm of these activity coefficients is considered to linearly depend on the fraction of oxidized sites and therefore the Nernst equation can be written as:

$$E = E^{0\prime} + \frac{RT}{F}\ln\left(\frac{f_{Ox}}{1-f_{Ox}}\right) - \frac{RT}{F}\Gamma_{Os} f_{Ox} r \tag{20}$$

where $E^{0\prime}$ is the redox potential of the couple (a fitting parameter), f_{Ox} is the fraction of oxidized sites, Γ_{Os} is the surface coverage of osmium sites and r is an interaction parameter (which is equal to $r_O + r_R$ in Anson's original work). The

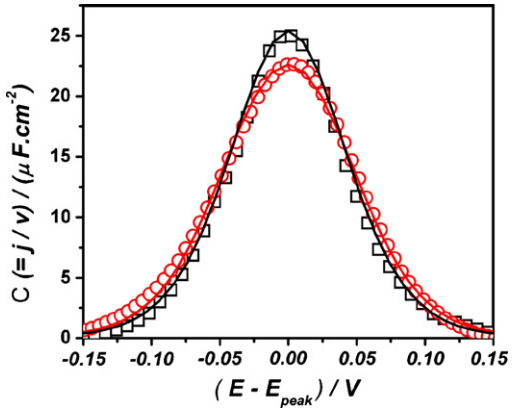

Fig. 7. Baseline subtracted experimental redox waves for experiments performed at $C_S = 1$ mM (squares) and $C_S = 1.2$ M (circles) in the same conditions of Fig. 2. The best-fit curve to the lateral interaction model of Eq. (20) is shown in solid lines. The best-fit parameters are $r = -6.0 \times 10^9$ cm^2 mol^{-1} ($C_S = 1.2$ M) and -15.0×10^9 cm^2 mol^{-1} ($C_S = 1$ mM) and $\Gamma_{Os} = 2.94 \times 10^{-11}$ mol cm^{-2}.

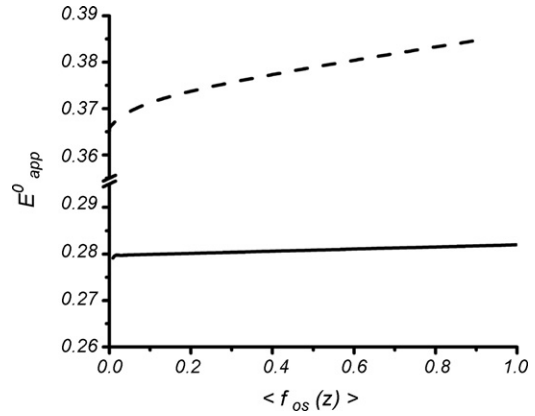

Fig. 8. Formal (apparent) Os(III)/Os(II) redox potential as a function of the average fraction of oxidized osmium sites for the two ionic strengths employed in Fig. 7, 1 mM (dashed line) and 1.2 M (solid line) and pH 3. The lateral interaction parameters, r, determined from the slope of the plot (according to Eq. (22)) are -3.4×10^9 cm^2 mol^{-1} ($C_S = 1.2$ M) and -22.0×10^9 cm^2 mol^{-1} ($C_S = 1$ mM).

capacitance–potential curve in this model is given by:

$$\frac{i}{v} = \frac{n^2F^2\Gamma_{Os}}{RT}\frac{f_{Ox}(1-f_{Ox})}{1 - f_{Ox}\Gamma_{Os} r(1-f_{Ox})} \tag{21}$$

Best fits parameters for r in Fig. 7 are -6.0×10^9 cm^2 mol^{-1} ($C_S = 1.2$ M) and -15.10^9 cm^2 mol^{-1} ($C_S = 1$ mM) and $\Gamma_{Os} = 2.94 \times 10^{-11}$ mol cm^{-2}. As expected, the interactions are stronger for the lower ionic strength solution.

The molecular theory explicitly considers the local activity of all the species in the system. The mathematical dependence of the activity coefficients for the osmium sites with the oxidation fraction is not restricted to that supposed by Brown and Anson, however our calculations can be used to predict the interaction parameter of that model without the need of fitting the experimental data. In order to do that, we should first define the apparent redox potential of the couple, E^0_{app} as the standard redox potential of the couple plus the electrochemical activity term, from Eq. (20) we have:

$$E^0_{app} = E^{0\prime} - \frac{RT}{F} r\Gamma_{Os} f_{ox} \tag{22}$$

It is a common practice in electrochemistry to rewrite the Nernst equation in terms of concentrations instead of activities using the formal or conditional potential:

$$E = E^0_{app} + \frac{RT}{F}\ln\left(\frac{f_{Ox}}{1-f_{Ox}}\right) \tag{23}$$

Since the molecular theory provides us with a distance dependent oxidation fraction, the fraction of oxidized sites f_{Ox} is equal to the average oxidation fraction; $\langle f_{Os}\rangle$ defined as:

$$\langle f_{Os}\rangle = f_{Ox} = \frac{\int \langle n_{Os}(z)\rangle\, f_{Os}(z)\, dz}{\int \langle n_{Os}(z)\rangle\, dz} \tag{24}$$

We can now determine E^0_{app} for a given electrode potential and Eq. (23). The interaction parameters, r can be estimated from the slope of a E^0_{app} vs. $\langle f_{Os}\rangle$ plot (see Eq. (22) and Fig. 8). The results obtained for r are -3.4×10^9 cm^2 mol^{-1} ($C_S = 1.2$ M)

Table 3
Peak width for electrolytes of different concentration, C_S and pH 3

C_S (M)	Experimental FWHH (V)	Theoretical FWHH (V)
0.004	0.104	0.106
0.02	0.102	0.106
0.04	0.102	0.104
0.08	0.100	0.100
0.12	0.099	0.098
0.16	0.099	0.096
0.2	0.097	0.095
0.3	0.096	0.094
0.4	0.095	0.093
0.5	0.095	0.093
0.8	0.094	0.093
1.2	0.093	0.093

and -22.0×10^9 cm^2 mol^{-1} ($C_S = 1$ mM), are in good agreement with those determined by the Anson method from Fig. 7. Note that the curve in Fig. 8 departs from the Brown and Anson model (linear behavior) at reductive potentials.

A simpler way to study lateral interactions in these films is by directly studying the peak FWHH. Table 3 shows a comparison between experimentally measured and theoretically predicted FWHH for solutions of different ionic strength, with very good agreement between theory and experiment.

An interesting consequence of the coupling that exists in the molecular theory between the chemical equilibria, the spatial distribution of mobile ions and the interaction fields is the ability of the system to regulate its own charge as a response to a change in the experimental variables. As an example, increasing the bulk pH leads to amine deprotonation, which in turn decreases the electrostatic potential in the film and stabilizes Os(III) over Os(II). This effect causes the decrease in the apparent redox potential in alkaline solutions shown in Fig. 5. In Fig. 9A, we show the average fraction of oxidized osmium groups (given by Eq. (24)) as a function of the electrode potential for pH 3 (protonated film) and pH 13 (deprotonated film) electrolyte solutions. This plot shows how the standard potential of the couple is affected by bulk pH. Furthermore, during film oxidation the electrostatic potential in the film increases and triggers amine deprotonation. This effect is shown in Fig. 9B, which depicts the average fraction of charged amino groups, $\langle f_c \rangle$ (defined in analogy with Eq. (24)) as a function of bulk pH for totally reduced ($E = 0$ V) and totally oxidized ($E = 0.6$ V) films. The apparent pK_a for the amines in the film (defined as the pH where $\langle f_c \rangle = 0.5$) depends therefore on the oxidation state of the film. The dependence is not very pronounced because the film contains much less osmium sites than amines.

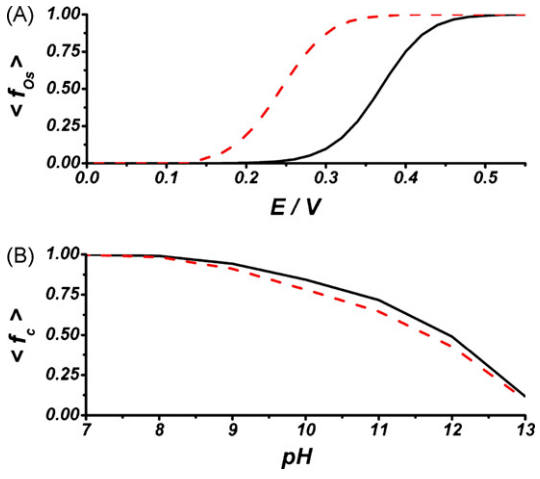

Fig. 9. (A) Average fraction of oxidized osmium sites as a function of electrode potential for pH 3 (solid line, $E^0_{app} = 0.368$ V) and pH 13 (dashed line, $E^0_{app} = 0.244$ V). (B) Average fraction of protonated amine groups as a function of pH for $E = 0$ V (solid line, p$K_a^{app} = 11.9$) and $E = 0.6$ V (dashed line, p$K_a^{app} = 11.7$). Salt concentration was 4 mM in all calculations.

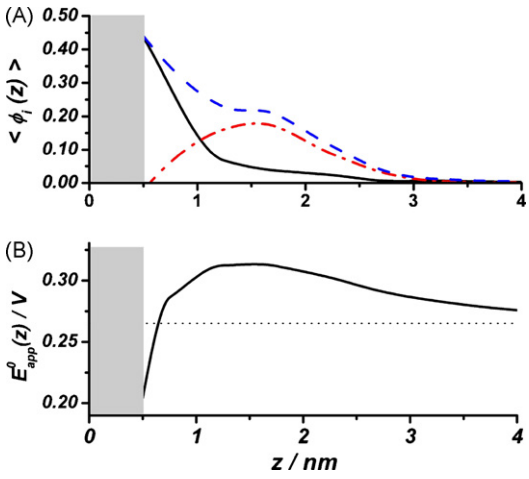

Fig. 10. (A) Theoretical volume fraction profiles for the polymer backbone (full line), the redox sites (dot-dashed line) and the whole redox polymer (dashed line) calculated at $E = E^0_{Os(II)/Os(III)}$ using $C_{salt} = 0.1$ M and pH 3. The shaded region ($z < 0.5$ nm) is occupied by the thiol layer. (B) Distance dependant formal Os(III)/Os(II) redox potential as a function of the distance from the electrode (solid curve) calculated for the same experimental conditions than A.

The molecular theory allows us to make predictions on the structure and organization of the electrode/PAH-Os/electrolyte interface and how it depends on the experimental conditions. As an example we show in Fig. 10A the volume fraction for the redox polyelectrolyte and of its two components, the redox groups and the polymeric backbone, as a function of the distance from the electrode. The calculations shows that the redox polymer is strongly adsorbed and constrained to 2 nm from the metal surface. The osmium complexes are segregated from the interface due to it bulky nature. The polymer volume fraction does not became zero until approximately 12 nm because of the presence of dangling tails which adopt extended conformations in order to minimize electrostatic repulsions. We have observed that the volume fraction profile of these tails is very sensitive to electrolyte pH and ionic strength. For comparison with experiments, the structural information can be resumed in a theoretical film thickness (calculated as the first moment of the volume fraction distribution of the polymers [60]) which can be thereafter contrasted with the experimental ellipsometric thickness. We found that the ellipsometric thickness in 0.2 M KNO_3 pH 7.3 buffer solution of 1.5 nm is consistent with the theoretical prediction for the same conditions of 1.2 nm.

Not only the distribution of the redox polymer across the interface is highly inhomogeneous, but also its properties are

also very dependant on the distance from the electrode. As an example, in Fig. 10B we show the formal (apparent) redox potential profile for the osmium couple, which we define at each z as the standard electrode potential plus the electrochemical activity term at z:

$$E^0_{app}(z) = E^{0,abs}_{Os(III)/Os(II)} + \frac{(q_{ox} - q_{red})}{|e|}\psi(z) \quad (25)$$

While Eqs. (12) and (25) show that the activity term depends on the local electrostatic potential at z, $\psi(z)$, this interaction field is affected by the distribution of all the species in the system. These distributions are in turn determined from all the interaction forces and chemical equilibria included in the theory. The second term in the right-hand side of Eq. (25) should therefore be regarded as a non-local activity term including all the possible interactions.

We have defined an average formal potential E^0_{app} from the Nernst equation (see Eq. (23)). This average formal potential results from the contribution from osmium sites located at different distances from the electrode, having a local formal potential $E^0_{app}(z)$. Note however that the average potential is defined from the average fraction of oxidized sites and therefore it is not equal to the weighted average of the z-depended formal potential defined in Eq. (25). The calculated E^0_{app} for the conditions in Fig. 10B is 0.305 V, thus comparison between Fig. 10A and B clearly shows that the local formal potential of those regions having a higher local concentration of osmium sites have a larger impact on E^0_{app}. Fig. 10B introduces the interesting concept of a z-dependent distribution of redox formal potentials.

4. Conclusions

We have employed a molecular theory to describe a thiolated gold electrode modified by an ultrathin layer of a redox polyelectrolyte (PAH-Os). The theory explicitly incorporates the different inter and intramolecular interactions and thus it accounts for the size, shape, conformations, charge, and charge distribution of all of the molecular species in the film.

The theory predicts the molecular organization of the interface and the equilibrium electrochemistry for a given experimental condition. Within the molecular structural description the theory provides for a detailed picture of the highly inhomogeneous distribution of all the molecular species as well as the distance dependent acid–base equilibrium and redox states. The results of the calculations show that the variation of the redox and charge states within a thin film is quite pronounced.

Experimental low scan rate current–potential curves for solutions of different pH and ionic strength are in good agreement with capacitance–potential curves calculated with the molecular theory without the use of any adjustable parameter. The theory provides a link between the molecular organization of the film and the electrochemical behavior. The good agreement between the predicted electrochemistry and the experimentally measured scans provides support that the structural features predicted from the theory, and that cannot be measured directly, are correct.

The analysis of peak potential, FWHH, dependence on ionic strength and pH with phenomenological models from the literature has been carried out and fitted values for the unknown parameters have been obtained. For example, the charge obtained from the Donnan and from the Gouy-Champman models are close to each other. This value is also close to the one obtained from the molecular theory. However, the molecular theory provides the whole charge distribution and it demonstrates that the resulting charge results from strong charge regulation of the sulfonate groups. This implies that the physical picture representing the experimental situation (as explained from the molecular theory) is rather different than the conclusions that would be obtained from the simpler phenomenological models. The same type of conclusion is obtained by fitting the interaction parameter from the Brown Anson model to the experimental data. The best fit provides an average value for the interactions, that is in line with that predicted from the molecular theory. The difference is that the molecular approach shows that this average value is the result of a complex set of interactions that are determined by the structure of the film.

To summarize, the phenomenological models provide with a set of fitting parameters that while reliable cannot be used to predict the behavior of a system that has not been studied experimentally. Moreover, their application, while simple, does not provide for a molecular picture of the relationship between structure and electrochemical behavior and the very important coupling that exists between the different interactions and the variation of redox and charge state of the different components of the film. The molecular theory provides a very detailed molecular picture and each of the contributions can be determined explicitly. Furthermore, the very good agreement with the experimental observations without the use of adjustable parameters demonstrates the predictive power of the theory. Thus, we can use this approach as a design tool and at the same time obtain fundamental understanding of the main factors that determine the experimentally observed behavior. It should be stressed that the theory still contains several approximations, however, we believe that they are appropriate to treat polymer-modified electrodes based on the results presented here and in our previous work. The main backdrop of the theory is that the calculations are non-trivial and the calculations are explicitly dependent on the specific chemical nature of the molecules composing the system.

The phenomenological theories provide with simple expressions but very limited (or none) molecular understanding of the observed behavior. Paying the price of a more complex calculation with the molecular theory provides a wealth of first principle predictions for both the structural, thermodynamic and equilibrium electrochemical behavior of the films. We plan to extend the theory in future work to include dynamic effects.

Acknowledgements

E.J.C. and M.T. acknowledge financial support from CONICET (Argentina), the University of Buenos Aires, and ANPCyT (BID 1728 OC-AR PICT 2003 No. 06-17170). M.T. has a cooperative CONICET-FUDETEC industrial research grant. E.J.C. is a permanent research staff of CONICET. I.S. acknowledges

the financial support from the National Science Foundation of the United States.

References

[1] B.E. Conway, Theory and Principles of Electrode Processes, 1st ed., The Ronald Press Co, New York, 1965.
[2] R.A. Marcus, Angewandte Chemie International Edition 32 (1993) 1111.
[3] J. Wass, E. Ahlberg, I. Panas, D. Schiffrin, PCCP 8 (2006) 4189.
[4] J. Wass, E. Ahlberg, I. Panas, D. Schiffrin, J. Phys. Chem. A 110 (2006) 2005.
[5] A.J. Bard, L.R. Faulkner, Electrochemical Methods: Fundamentals and Applications, 2nd ed., John Wiley & Sons, New York, 2001.
[6] M.E.G. Lyons, Electroactive Polymer Electrochemistry, 1, Plenum Press, New York, 1994.
[7] G. Decher, Science 277 (1997) 1232.
[8] G. Decher, in: G. Decher, B.J. Schlenoff (Eds.), Multilayer Thin Films, Wiley-VCH, Weinheim, 2003.
[9] Y. Lvov, G. Decher, G. Sukhorukov, Macromolecules 26 (1993) 5396.
[10] J.B. Schlenoff, H. Ly, M. Li, J. Am. Chem. Soc. 120 (1998) 7626.
[11] J. Stepp, J.B. Schlenoff, J. Electrochem. Soc. 144 (1997) 155.
[12] T. Fushimi, A. Oda, H. Ohkita, S. Ito, Thin Solid Films 484 (2005) 318.
[13] J. Hodak, R. Etchenique, K. Singhal, P.N. Bartlett, E.J. Calvo, Langmuir 13 (1997) 2708.
[14] S.F. Hou, H.Q. Fang, H.Y. Chen, Anal. Lett. 30 (1997) 1631.
[15] A. Liu, J. Anzai, Langmuir 19 (2003) 4043.
[16] A. Liu, Y. Kashiwagi, J. Anzai, Electroanalysis (2003).
[17] V. Rosca, I.C. Popescu, Electrochem. Commun. 4 (2002) 904.
[18] H.C. Yoon, M.Y. Hong, H.S. Kim, Anal. Chem. 72 (2000) 4420.
[19] H.C. Yoon, H.S. Kim, Anal. Chem. 72 (2000) 922.
[20] E.J. Calvo, A. Wolosiuk, J. Am. Chem. Soc. 124 (2002) 8490.
[21] E.J. Calvo, F. Battaglini, C. Danilowicz, A. Wolosiuk, M. Otero, Faraday Discuss. (2000) 47.
[22] E.J. Calvo, A. Wolosiuk, ChemPhysChem 5 (2004) 235.
[23] E.J. Calvo, C. Danilowicz, A. Wolosiuk, J. Am. Chem. Soc. 124 (2002) 2452.
[24] E.J. Calvo, C.B. Danilowicz, A. Wolosiuk, PCCP 7 (2005) 1800.
[25] E.J. Calvo, R. Etchenique, L. Pietrasanta, A. Wolosiuk, Anal. Chem. 73 (2001) 1161.
[26] E.S. Forzani, M. Otero, M.A. Pérez, M. López Teijelo, E.J. Calvo, Langmuir 18 (2002) 4020.
[27] E.S. Forzani, M.A. Perez, M.L. Teijelo, E.J. Calvo, Langmuir 18 (2002) 9867.
[28] N. Sarkar, M. KuRam, A. Sarkar, R. Narizzano, S. Paddeu, C. Nicolini, Nanotechnology 11 (2000) 30.
[29] R.W. Murray, Acc. Chem. Res. 13 (1980) 135.
[30] R.W. Murray, in: R.W. Murray (Ed.), Molecular Design of Electrode Surfaces, John Wiley and Sons, Inc., New York, 1992.
[31] R.W. Murray, A.G. Ewing, R.A. Durst, Anal. Chem. 59 (1987) A379.
[32] S. Srinivasan, M. Gileadi, Electrochim. Acta 11 (1966) 321.
[33] E. Laviron, J. Electroanal. Chem. 100 (1979) 263.
[34] E. Laviron, J. Electroanal. Chem. 112 (1980) 1.
[35] E. Laviron, J. Electroanal. Chem. 124 (1981) 9.
[36] A.P. Brown, F.C. Anson, Anal. Chem. 49 (1977) 1589.
[37] W.J. Albery, M.G. Boutelle, P.J. Colby, A.R. Hillman, J. Electroanal. Chem. 133 (1982) 135.
[38] C.E.D. Chidsey, R.W. Murray, J. Phys. Chem. 90 (1986) 1479.
[39] E.F. Bowden, M.F. Dautartas, J.F. Evans, J. Electroanal. Chem. Interfacial Electrochem. J219 (1987) 91.
[40] C.P. Andrieux, J.M. Savéant, J. Phys. Chem. 92 (1988) 6761.
[41] D.N. Blauch, J.M. Savéant, J. Phys. Chem. 97 (1993) 6444.
[42] D.N. Blaunch, J.M. Savéant, J. Am. Chem. Soc. 3323 (1992).
[43] J.M. Savéant, J. Phys. Chem. 92 (1988) 4526.
[44] K. Doblhofer, M. Vorotyntsev, in: M.E.G. Lyons (Ed.), Electroactive Polymer Electrochemistry, Plenum, New York, 1994, p. 375.
[45] R. Naegeli, J. Redepenning, F.C. Anson, J. Phys. Chem. 90 (1986) 6227.
[46] J. Redepenning, F.C. Anson, J. Phys. Chem. 91 (1987) 4549.
[47] J. Redepenning, B.R. Miller, S. Burham, Anal. Chem. 66 (1994) 1560.
[48] H. Ohshima, S. Ohki, Biophys. J. 47 (1985) 673.
[49] M. Tagliazucchi, F. Williams, E.J. Calvo, J. Phys. Chem. B 111 (2007) 8105.
[50] C.P. Smith, H.S. White, Langmuir 9 (1993) 1.
[51] H.S. White, J.D. Peterson, Q. Cui, K.J. Stevenson, J. Phys. Chem. B 102 (1998) 2930.
[52] M. Bryant, R.M. Crooks, Langmuir 9 (1993) 385.
[53] I. Burgess, B. Seivewright, R.B. Lennox, Langmuir 22 (2006) 4420.
[54] W.R. Fawcett, M. Fedurco, Z. Kováčová, Langmuir 10 (1994) 2403.
[55] R. Andreu, W.R. Fawcett, J. Phys. Chem. 98 (1994) 12753.
[56] R. Andreu, J.J. Calvente, W.R. Fawcett, M. Molero, Langmuir 13 (1997) 5189.
[57] D. Posadas, M. Fonticelli, M.J.R. Presa, M.I. Florit, J. Phys. Chem. B 105 (2001) 2291.
[58] D. Posadas, M.I. Florit, J. Phys. Chem. B 108 (2004) 15470.
[59] L. Lizarraga, E.M. Andrade, M.I. Florit, F.V. Molina, J. Phys. Chem. B 109 (2005) 18815.
[60] M. Tagliazucchi, E.J. Calvo, I. Szleifer, J. Phys. Chem. C 112 (2007).
[61] I. Szleifer, M.A. Carignano, Adv. Chem. Phys. 94 (1996) 165.
[62] P. Gong, J. Genzer, I. Szleifer, Phys. Rev. Lett. 98 (2007) 018302.
[63] M. Carignano, I. Szleifer, J. Chem. Phys. 100 (1994) 3210.
[64] S. Trasatti, Pure & Appl. Chem. 58 (1986) 956.
[65] S. Trassati, J. Electroanal. Chem. 54 (1974) 19.
[66] C. Mokrani, J. Fatisson, L. Guerente, P. Labbe, Langmuir 21 (2005) 4400.
[67] R. Nap, P. Gong, I. Szleifer, J. Polym. Sci., Part B: Polym. Phys. 44 (2006) 2638.
[68] P.J. Flory, Principles of Polymer Chemistry, Cornell University Press, Ithaca, NY, 1953.
[69] CRC Handbook of Chemical and Physics, 72nd ed., CRC Press, Boston, 1991.
[70] M. Tagliazucchi, E.J. Calvo, I. Szleifer, Langmuir (in press), available in the web, doi:10.1021/la702734.

Glossary

N_P/A: number of polymer chains per unit area
N_{MPS}/A: number of thiol molecules per unit area
β: inverse temperature, $(k_B T)^{-1}$.
k_B: Boltzmann constant
e: elemental charge
F: Faraday constant
K_b^0: Thermodynamic equilibrium constant for amine deprotonation
$K_{a,MPS}^0$: Thermodynamic equilibrium constant for thiol sulfonate protonation
$E_{Os(II)/Os(III)}^{0,abs}$: Standard reduction potential for the Os(II)/Os(III) couple in PAH-Os
v_i: molecular volume of the species i (i = w, H^+, OH^-, C, A for water molecules, proton, hydroxyls, cations and anions, respectively)
q_i: charge of the species i in units of elemental charge
$\rho_i(z)$: number density of species i at z
$\phi_i(z)$: volume fraction of the species i at z
$P_P(\alpha)$: probability of having a polymer chain in the conformation α
$P_{MPS}(\gamma)$: probability of having a thiol chain in conformation γ
$f_c(z)$: fraction of charged amino groups at z
$\langle f_c \rangle$: average fraction of charged amino groups
$\Delta_{ox}\langle f_c \rangle$: change in the average fraction of charged amino groups upon oxidation
$f_{c,MPS}(z)$: fraction of charged sulfonate groups at z
$\langle f_{c,MPS} \rangle$: average fraction of charged sulfonate groups
$\Delta_{ox}\langle f_{c,MPS} \rangle$: change in the average fraction of charged sulfonate groups upon oxidation
$\langle z \rangle$: average film thickness
$\Delta_{ox}\langle z \rangle$: change in the average film thickness upon oxidation
$f_{Os}(z)$: fraction of oxidized osmium sites at z
$n_P(z, \alpha)$: number of polymer allylamine segments that a chain in conformation α has at z
$n_{Os}(z, \alpha)$: number of osmium sites that a chain in conformation α has at z

$v_P(z, \alpha)$: volume occupied at z by polymer segments for a chain in conformation α.

$v_{Os}(z, \alpha)$: volume occupied at z by the redox sites for chain in conformation α

$\langle n_P(z)\rangle$: average density of polymer segments at z, $\sum_{\alpha} P_{\mathrm{P}}(\alpha) n_{\mathrm{P}}(z, \alpha)$

$\langle n_{MPS}(z)\rangle$: average density of thiols at z

$\langle n_{Os}(z)\rangle$: average density of redox sites at z, $\sum_{\alpha} P_{\mathrm{P}}(\alpha) n_{\mathrm{Os}}(z, \alpha)$

$\langle \phi_P(z)\rangle$: average volume fraction occupied by the polymer backbone at z, $\sum_{\alpha} P_{\mathrm{P}}(\alpha) \nu_{\mathrm{P}}(z, \alpha)$

$\langle \phi_{MPS}(z)\rangle$: average volume fraction occupied by the thiol at z

$\langle \phi_{Os}(z)\rangle$: average volume fraction of osmium sites at z, $\sum_{\alpha} P_{\mathrm{P}}(\alpha) \nu_{\mathrm{Os}}(z, \alpha)$

E_{eq}^{abs}: electrode potential of the metal in the absolute scale

E: electrode potential against Ag/AgCl reference electrode

σ_M: electrostatic charge on the metal

C_{redox}: electrode redox capacitance

$C_{non\text{-}redox}$: electrode non-redox capacitance

$\chi(|z - z'|)$: distance dependent vdW interaction parameter

$\psi(z)$: (outer) electrostatic potential at z

$\varepsilon(z)$: z-dependent dielectric coefficient

$\langle \rho_Q(z)\rangle$: average density of charges at z

$U_{PS}(\alpha)$: van der Waals interaction energy between the surface and a polymer chain in conformation α

μ_i^0: standard chemical potential for the species i participating in a chemical equilibrium

μ_i: chemical potential for a mobile species i

$\pi(z)$: Lagrange multiplier enforcing the packing constraint at z (lateral osmotic pressure)

λ: Lagrange multiplier assuring global electroneutrality (additive constant to the electrostatic potential)

ξ: normalization constant assuring $\sum_{\alpha} P(\alpha) = 1$